

# Geophysical Research Letters<sup>®</sup>



## RESEARCH LETTER

10.1029/2025GL114712

### Key Points:

- The Cross-track infrared sounder (CrIS) instrument detected high tropical isoprene anomalies in 2020
- Increasing isoprene emissions to match CrIS results in better agreement with MOPITT CO and interhemispheric OH parity
- This isoprene anomaly could have contributed to 13% (10%–28%) of 2020's methane growth if driven by isoprene emissions

### Supporting Information:

Supporting Information may be found in the online version of this article.

### Correspondence to:

A. J. Turner,  
[turneraj@uw.edu](mailto:turneraj@uw.edu)

### Citation:

Yoon, J. (Y. S.), Wells, K. C., Millet, D. B., Swann, A. L. S., Thornton, J., & Turner, A. J. (2025). Impacts of interannual isoprene variations on methane lifetimes and trends. *Geophysical Research Letters*, 52, e2025GL114712. <https://doi.org/10.1029/2025GL114712>

Received 7 JAN 2025

Accepted 30 JUN 2025

### Author Contributions:

**Conceptualization:** James (Young Suk) Yoon, Abigail L. S. Swann, Joel Thornton, Alexander J. Turner

**Data curation:** Kelley C. Wells, Dylan B. Millet

**Formal analysis:** James (Young Suk) Yoon, Joel Thornton, Alexander J. Turner

**Funding acquisition:** Alexander J. Turner

**Investigation:** James (Young Suk) Yoon, Abigail L. S. Swann, Joel Thornton, Alexander J. Turner







**Methodology:** James (Young Suk) Yoon, Kelley C. Wells, Dylan B. Millet, Abigail L. S. Swann, Joel Thornton, Alexander J. Turner

**Resources:** Alexander J. Turner

© 2025 The Author(s).

This is an open access article under the terms of the [Creative Commons Attribution-NonCommercial](https://creativecommons.org/licenses/by-nc/4.0/) License, which permits use, distribution and reproduction in any medium, provided the original work is properly cited and is not used for commercial purposes.

## Impacts of Interannual Isoprene Variations on Methane Lifetimes and Trends

James (Young Suk) Yoon<sup>1</sup> , Kelley C. Wells<sup>2</sup> , Dylan B. Millet<sup>2</sup> , Abigail L. S. Swann<sup>1,3</sup> , Joel Thornton<sup>1</sup> , and Alexander J. Turner<sup>1</sup> 

<sup>1</sup>Department of Atmospheric and Climate Science, University of Washington, Seattle, WA, USA, <sup>2</sup>Department of Soil, Water and Climate, University of Minnesota, Falcon Heights, MN, USA, <sup>3</sup>Department of Biology, University of Washington, Seattle, WA, USA

**Abstract** Recent observations show anomalously high methane growth in 2020, which has been attributed to increased wetland emissions and decreased OH from lower COVID-19 nitrogen oxide (NO<sub>x</sub>) emissions. NO<sub>x</sub> is not the only species that affects OH—isoprene, the most significant non-methane hydrocarbon by total emissions, is oxidized by OH, which can deplete OH during periods of high emissions. Using satellite isoprene retrievals from the Cross-track infrared sounder (CrIS), we find anomalously high isoprene columns during 2020, coincident with high methane growth. Isoprene's oxidation produces carbon monoxide, which can be transported over longer distances and decrease OH outside of isoprene source regions. Elevated isoprene concentrations may have contributed 13% (bounds: 10%–28%) of 2020's methane growth if we assume no change in NO<sub>x</sub> emissions in 2020. Since COVID-19 decreased anthropogenic NO<sub>x</sub> emissions, this estimate is an upper-limit and may depend on whether isoprene or NO emissions drove this isoprene anomaly.

**Plain Language Summary** Methane is a potent greenhouse gas and a major contributor to global warming. In 2020, there was an unprecedented rise in methane concentrations that has often been attributed to changes in methane emissions or changes in oxidant levels from the COVID-19 pandemic. Here, we use novel satellite measurements of isoprene, an organic compound emitted by trees, to suggest that the biosphere may have contributed to some of these recent methane trends through changes in oxidant levels, potentially affecting methane loss in the atmosphere.

## 1. Introduction

Methane (CH<sub>4</sub>) is the second most important greenhouse gas behind carbon dioxide and is 84 times more potent than carbon dioxide over a 20-year time horizon (Smith et al., 2021). It is emitted from natural and anthropogenic sources, including oil and gas infrastructure, coal mining, rice cultivation, landfills, feedlots, and wetlands, while its dominant sink is oxidation initiated by the hydroxyl (OH) radical with a lifetime of 9–12 years (Saunois et al., 2020). Thus, variations in both methane emissions and OH concentrations, [OH], can impact observed methane mixing ratios. The latter may have been important for the rising methane mixing ratios observed after 2007, which previous work has attributed to decreased [OH] and an increase in the methane lifetime, among other hypotheses (e.g., Turner et al., 2017; Rigby et al., 2017).

In 2020 and 2021, global methane mixing ratios grew at unprecedented rates (hereby referred to as “methane acceleration”). Previous studies attributed this trend to increased emissions (Hardy et al., 2023) or decreased [OH] from lower nitrogen oxide (NO<sub>x</sub>) emissions during the COVID-19 lockdowns (Laughner et al., 2021). Peng et al. (2022) attributed the methane acceleration to both increased wetland emissions and decreased [OH] due to NO<sub>x</sub> changes during the COVID-19 pandemic, with a [OH] decrease of  $1.6 \pm 0.2\%$  contributing to  $53 \pm 10\%$  of the observed methane trend. Other studies argue that the methane acceleration was largely due to wetland emissions with little impact from OH changes: for example, Feng et al. (2023) attributed just 16% of the acceleration to OH.

NO<sub>x</sub> emissions are not the only factor determining tropospheric [OH] and the global methane sink: global [OH] also generally increases with actinic flux, tropospheric ozone, and atmospheric water vapor, and decreases with volatile organic compound (VOC) emissions. Isoprene is a biogenic VOC (BVOC) released largely from broadleaf deciduous trees in response to high light and temperature conditions (Bamberger et al., 2017; Velikova et al., 2011; Zheng et al., 2017) in large enough quantities to potentially affect global [OH]. By total flux, isoprene

**Supervision:** Joel Thornton, Alexander J. Turner

**Validation:** Kelley C. Wells, Dylan B. Millet

**Visualization:** James (Young Suk) Yoon, Alexander J. Turner

**Writing – original draft:** James (Young Suk) Yoon

**Writing – review & editing:** James (Young Suk) Yoon, Kelley C. Wells, Dylan B. Millet, Abigail L. S. Swann, Joel Thornton, Alexander J. Turner

is the most significant non-methane VOC, with estimates of 440–660 Tg C yr<sup>−1</sup> emitted into the atmosphere as isoprene (A. Guenther et al., 2006). Once in the atmosphere, isoprene is predominantly oxidized by OH, with typical lifetimes on the order of 1 hr, creating organic products like isoprene epoxydiols that are involved in photochemical smog and secondary organic aerosol formation (Bates & Jacob, 2019; Kroll et al., 2006). Due to its large reaction rate constant toward OH, high isoprene emissions can deplete local [OH], which in turn can extend isoprene's own lifetime. For example, implementing isoprene chemistry via the reduced Caltech isoprene mechanism into the chemical transport model GEOS-Chem resulted in 70% reductions to local [OH] in the Amazon and equatorial Africa, as well as a 12% increase in the tropospheric methane lifetime (Bates & Jacob, 2019). Isoprene impacts are therefore not restricted to its source regions but can impact global [OH]. As isoprene emissions are driven by ecosystem characteristics, regional climate, and weather, global [OH] variability can therefore be due in part to processes that alter isoprene emissions.

Isoprene emissions in chemical transport (e.g., GEOS-Chem) or chemistry-enabled climate models (e.g., CAM6-Chem) are often parameterized through MEGAN (Model of Emissions of Gases and Aerosols from Nature) v2.1, which calculates isoprene emissions as the product of a vegetation-specific emission factor; the fractional area covered by that vegetation type; and an activity factor that accounts for isoprene's dependence to light, temperature, soil moisture, CO<sub>2</sub>, leaf age, and leaf area index (Emmons et al., 2020; A. Guenther et al., 2006; A. B. Guenther et al., 2012). To provide top-down space-based constraints on isoprene emissions, previous studies have traditionally used formaldehyde as an isoprene proxy, since formaldehyde is an isoprene oxidation product with a globally averaged yield of 22% per carbon (Bates & Jacob, 2019; Millet et al., 2006, 2008; Palmer et al., 2003, 2006). However, using formaldehyde as a proxy in low [OH] regions can result in smoothing caused by advection (Turner et al., 2012). In addition to smoothing, the formaldehyde yield from isoprene oxidation increases with local NO<sub>x</sub> concentrations, and fires or VOCs like methanol are other sources of formaldehyde that are independent of isoprene (Wolfe et al., 2016).

In 2020, Wells et al. developed novel isoprene satellite measurements from the Cross-track infrared sounder (CrIS) instrument using a brightness temperature difference and an artificial neural network; in 2022, this algorithm was revised to use a hyperspectral index (Shutter et al., 2024; Wells et al., 2020, 2022). Recently, these retrievals have been used to investigate multiyear trends in the atmospheric oxidative capacity over the South-eastern United States, and ENSO-driven OH variability in Papua New Guinea (Shutter et al., 2024).

The largest isoprene anomalies in the 9-year CrIS record occur in late-2019 and continue through 2020 (Figure 1a). This anomaly is not well-represented in GEOS-Chem with MEGAN-generated BVOC emissions (Figure 1a), and these isoprene column anomalies roughly coincide with the methane acceleration. Here we investigate whether elevated isoprene levels driven by higher isoprene emissions could indirectly contribute to the observed methane acceleration by modulating [OH].

## 2. Materials and Methods

### 2.1. Model Simulations

All model runs were conducted using GEOS-Chem v14.1.1 with offline BVOC emissions on a 4° latitude by 5° longitude grid, spanning an 8 year period from 2012 to 2020 to temporally coincide with the CrIS data set. The first 5 months (February–June 2012) were considered spin-up and were removed from the analysis. In total, three model simulations were conducted, as summarized in Table S1 of Supporting Information S1: (a) a baseline simulation with offline MEGAN emissions, (b) an isoprene climatology simulation that removed interannual variations in isoprene emissions by replacing isoprene emissions at each point with its 2012–2020 monthly offline MEGAN climatology (“isoprene\_climatology”), and (c) a simulation where isoprene emissions were scaled to better match the CrIS retrievals (“scaled\_isoprene”). Anthropogenic NO emissions were taken from the CEDSv2 inventory with 2020 anthropogenic NO emissions set at 2019 emissions, as 2020 data was not available at the time of the runs. Isoprene chemistry was parametrized using the Bates and Jacob (2019) mechanism. Texts S1–S3 in Supporting Information S1 describe the satellite measurements used in this study.

For simulation 3 (“scaled\_isoprene”), we iteratively scaled isoprene emissions to better match the CrIS retrievals. This iteration was necessary to account for the non-linear relationship between isoprene emissions and concentrations simulated by GEOS-Chem, due to isoprene's feedback on [OH]. Preliminary scalings indicated that a doubling of isoprene emissions over the Amazon and equatorial Africa resulted in a three-fold increase in

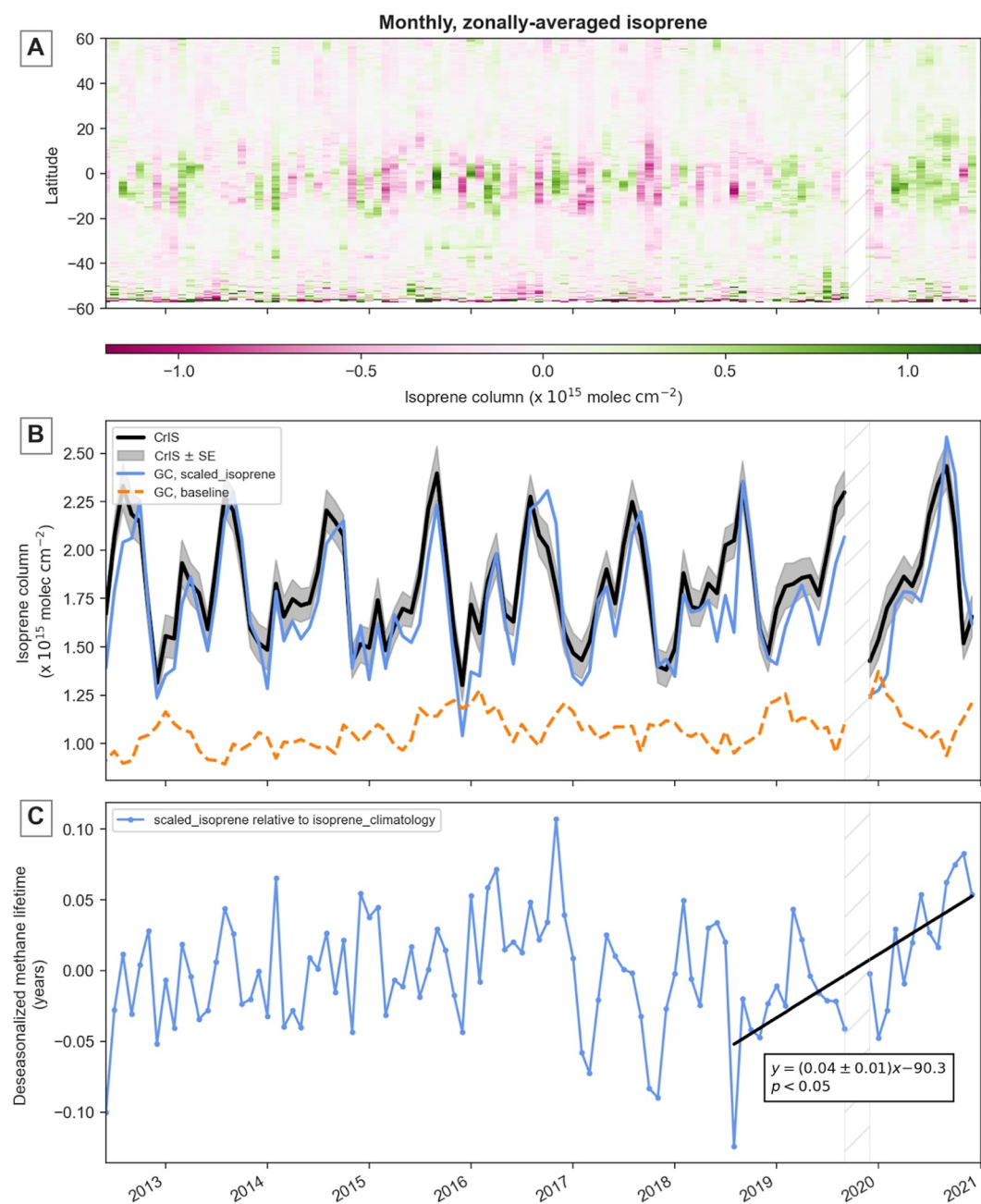


**Figure 1.** Time series analysis of isoprene and the methane lifetime. Hatched lines cover October–November 2019, which is due to anomalously high isoprene across all latitudes that may be an artifact of the background calculation — a copy of the figure without the hatching can be found in Figure S3 of Supporting Information S1. (a) Hovmöller diagram with CrIS isoprene anomalies at each latitude between July 2012 and December 2020. Each latitude gridbox spans  $0.5^\circ$ , and anomalies were calculated relative to a monthly climatology at each gridbox. (b) Time-series of globally averaged isoprene columns from the baseline GEOS-Chem run (dashed orange), scaled\_isoprene GEOS-Chem run (solid light blue), and the CrIS instrument (solid black). The base run underpredicted CrIS columns, while the scaled run brings GEOS-Chem more in alignment with satellite observations. Furthermore, the scaled\_isoprene run has a different seasonal cycle than the baseline run, with the former peaking in mid-year and the latter peaking in January. This new seasonal cycle in the scaled\_isoprene simulation better matches the CrIS measurements. (c) Methane lifetimes for the scaled\_isoprene (light blue) simulation relative to isoprene\_climatology, which had no interannual variations in isoprene emissions. The scaled run showed an increase in methane lifetimes in 2019 and 2020 that is coincident with the 2020 methane acceleration.

modeled isoprene columns, which was due to isoprene's feedback with local [OH]. As isoprene emissions increase, isoprene depletes local [OH], which increases its own lifetime. To account for this feedback, our first iteration (run 3a) scaled MEGAN isoprene emissions at each point for every month using Equation 1.

$$\eta_1 = 1 + \frac{1}{2} \left( \frac{\text{CrIS}_{\text{isoprene}}}{\text{GC}_{\text{base, isoprene}}} - 1 \right) \quad (1)$$

In Equation 1,  $\eta_1$  is the scaling factor for offline MEGAN emissions at each latitude-longitude,  $\text{CrIS}_{\text{isoprene}}$  is the CrIS isoprene column retrieval (in molecules  $\text{cm}^{-2}$ ), and  $\text{GC}_{\text{base, isoprene}}$  is the isoprene column simulated by the baseline GEOS-Chem run. This ensured emissions were only changed in regions with GEOS-Chem isoprene columns that deviated from CrIS observations. The  $\frac{1}{2}$  can be thought of as a “feedback” factor, originating due to the empirical 3:2 relationship between isoprene columns and emissions. Scaling factors were first calculated on GEOS-Chem's  $4^\circ \times 5^\circ$  grid and then bilinearly interpolated to match GEOS-Chem's  $0.5^\circ \times 0.625^\circ$  offline BVOC emissions. This first iteration generally overestimated isoprene, particularly in the Northern mid-latitudes.

The second iteration improved on the first iteration by considering regional changes in [OH]. For each geographical region delineated in Figure S1 of Supporting Information S1, the change in isoprene emissions ( $\eta_1$  in Equation 1) was compared to the corresponding change in modeled isoprene columns between the first iteration and the baseline simulation:

$$\eta_2 = \frac{\text{CrIS}_{\text{isoprene}}}{\text{GC}_{\text{base, isoprene}}} \times \frac{E_1/E_{\text{base}}}{C_1/C_{\text{base}}} \quad (2)$$

In Equation 2,  $E_1$  and  $E_{\text{base}}$  represent the isoprene emissions in the first iteration and in the baseline simulation, and  $C_1$  and  $C_{\text{base}}$  represent the modeled isoprene columns (in molecules  $\text{cm}^{-2}$ ) from those same runs. The ratio  $\left( \frac{E_1/E_{\text{base}}}{C_1/C_{\text{base}}} \right)$ , which is equivalent to  $\frac{\eta_1}{C_1/C_{\text{base}}}$ , was computed for every year and represents the increase in isoprene solely due to the isoprene-OH feedback (i.e., regional feedback factors). A sensitivity run that calculated this ratio monthly rather than annually overcompensated for these model-observation discrepancies, resulting in more isoprene column variability in the simulation relative to CrIS. More frequent calculation of this ratio may require additional scaling iterations to reach a stable result.

Deseasonalized isoprene anomalies were calculated for each run by subtracting the 2012–2020 monthly averaged isoprene from each measurement, which accounts for each simulation's seasonal cycle. To estimate uncertainty in the 2020 methane lifetime impact, we note that the uncertainty in simulation 3 largely originates from the regional feedback factors used in the second iteration, that is, the  $\left( \frac{E_1/E_{\text{base}}}{C_1/C_{\text{base}}} \right)$  ratio in Equation 2. This regional ratio serves a similar purpose to the global  $\frac{1}{2}$  factor present in Equation 1, as they both modulate the isoprene based on the OH feedback. We thus set the upper and lower bounds of isoprene's impact by scaling isoprene emissions again using Equation 1, but replacing the  $\frac{1}{2}$  global feedback factor with the 16th and 84th percentiles of the  $\left( \frac{E_1/E_{\text{base}}}{C_1/C_{\text{base}}} \right)$  ratios used in the second iteration. These corresponded to  $\frac{1}{6}$  and  $\frac{1}{2}$ , respectively (Figure S2 in Supporting Information S1), and so the first iteration (run 3a) served as the upper bound on isoprene emissions. Percentiles were calculated by compiling all feedback factors at every gridpoint between 2012 and 2020.

## 2.2. Modeling the Impact on Atmospheric Methane

To estimate isoprene's global impact on 2020's methane acceleration, we used a two-box  $\text{CH}_4$ -OH model to calculate hemispheric methane concentrations at various OH concentrations with interactive OH. Further information about the model and its data sets can be found in Turner et al. (2017) and Nguyen et al. (2020).

We parameterized methane emissions to be constant prior to 2007, followed by a linear increase between 2007 and 2019, and then constant in 2020. While keeping methane emissions at 2019 levels in 2020, we implemented a stepwise decrease in OH. The OH in the two-box model was reduced by the same percent decrease in column [OH] between 2020 and 2019, as calculated in GEOS-Chem, for the *scaled\_isoprene* run relative to *isoprene\_climatology*. This difference isolates the impact of isoprene emissions alone on the oxidative capacity. This output was compared to the simulated methane concentrations using Peng et al. (2022)'s 1.6%



decrease in OH, which was responsible for approximately half of the methane growth; a 3% decrease in OH, which should correspond to a scenario where the entire methane acceleration was caused by OH changes; and methane observations. The observed methane growth rate was calculated via the monthly difference between hemisphere-averaged NOAA surface flask observations (Lan et al., 2024). Sites were selected following Turner et al. (2017).

### 3. Results

CrIS measurements indicate a period of anomalously high isoprene in 2020, with anomalies calculated using the 2012–2020 monthly mean at each CrIS grid point as the climatology. Figure 1a is a Hovmöller diagram that shows that much of this isoprene increase was located in the tropics ( $-20$  to  $20^\circ$  latitude). Here, we investigate the impact this anomaly has on the oxidative capacity under the potential hypothesis that isoprene emissions drove this CrIS isoprene column anomaly. The potential impacts of  $\text{NO}_x$  emissions and isoprene- $\text{NO}_x$  interactions are discussed later and in Texts S4 and S5 of Supporting Information S1.

The baseline GEOS-Chem simulation underpredicted global isoprene observed from CrIS by 50%. Our isoprene emission scaling (*scaled\_isoprene*) increased simulated global land isoprene columns to better match CrIS satellite observations, as shown in Figure 1b. We note that GEOS-Chem global [OH] is 20% higher than [OH] obtained from methyl chloroform (MCF) inversions (Lin et al., 2024; Zhao et al., 2023). This global OH bias may explain part, but not all, of the model-satellite discrepancy, and the impact of this bias would depend on how this global OH bias translates over low- $\text{NO}_x$  tropical regions.

The *scaled\_isoprene* simulation also reproduced the Hovmöller diagram in Figure 1a, albeit with smaller magnitudes (Figure S4 in Supporting Information S1). The scaled isoprene rarely exceeded observed CrIS isoprene except in late 2016 and late 2020, and generally underestimated the early isoprene seasonal peak, which may be due to the isoprene-[OH] feedback ratio in the scaling being computed on yearly timescales. The discrepancy in modeled-observed isoprene was highest in 2015 and 2019. Nevertheless, the *scaled\_isoprene* run was generally able to reproduce the CrIS-derived isoprene record.

Additionally, scaling isoprene (*scaled\_isoprene*) also altered the modeled seasonal cycle to better match CrIS's seasonal cycle, largely due to increased isoprene emissions and stronger seasonal cycles in areas such as equatorial Africa, the Maritime Continent, and the Northern mid-latitudes (Figures S5–S7 in Supporting Information S1). It also decreased the impact of a simulated isoprene hotspot in the southwestern Amazon while increasing the influence of other regions in the Amazon basin, namely the northern Amazon. These spatial trends are consistent with results from Wells et al. (2020).

Methane lifetimes increased by up to 0.8 years between the *isoprene\_climatology* and the *scaled\_isoprene* runs (Figure S8 in Supporting Information S1). Due to isoprene's new seasonal cycle when emissions are scaled to match CrIS retrievals, the change in methane lifetimes also had an annual cycle which spiked in September and October. When this seasonal cycle is removed, we also find interannual variation in the methane lifetime (Figure 1c). In 2019 and 2020, higher methane lifetimes of up to an additional 0.1 years occurred in the *scaled\_isoprene* run that did not appear in the baseline run; this increase in the methane lifetime is due to increases in isoprene emissions in the Amazon, the Maritime Continent, and parts of Southeast Asia during 2020 (Figure S9 in Supporting Information S1). Although this isoprene-driven change in methane lifetimes is comparable in magnitude to other time periods (e.g., 2016), this 2019–2020 change represents a coherent, linear trend that is coincident with 2020's anomalously high methane growth.

#### 3.1. Role of Carbon Monoxide

The oxidation of isoprene produces a range of oxygenated organic carbon products, for example, formaldehyde, which in turn can be oxidized to form carbon monoxide (CO) and eventually  $\text{CO}_2$ . Here, we find that less than half of the global [OH] decrease is due to the direct oxidation of isoprene, but instead rather due to its subsequent oxidation products which are themselves removed by OH. Figure 2 shows the contribution of each species in the isoprene oxidation cascade to global OH depletion, with all column reaction rates reported as the difference between the *scaled\_isoprene* and *baseline* runs. We observe that 30%–70% of the increased oxidation is due to the  $\text{CO} + \text{OH}$  reaction, with its maximum fractional impact occurring during winter in the Northern Hemisphere. This finding is consistent with previous studies that show isoprene is a major contributor to the CO

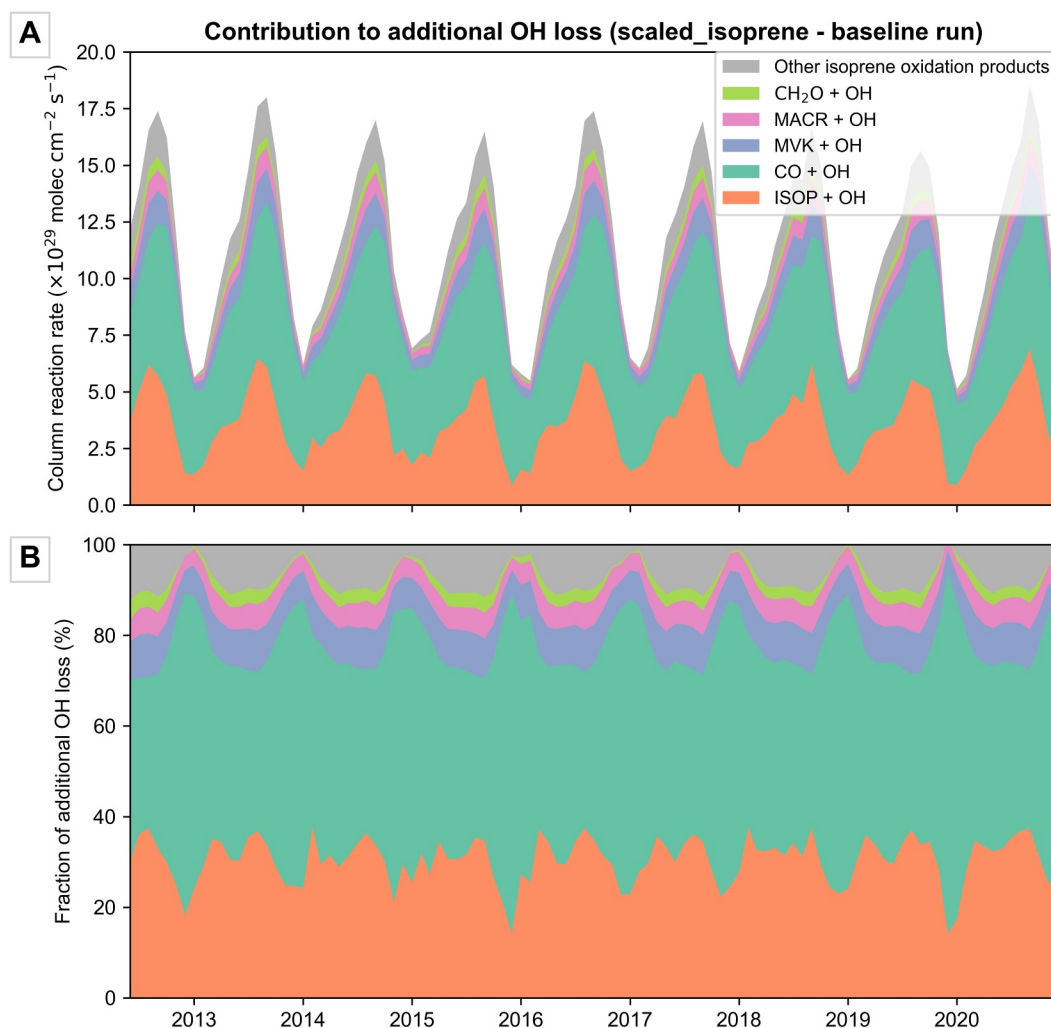


**Figure 2.** Contribution of various species to the global OH decrease observed between the scaled\_isoprene and baseline runs due to faster VOC + OH reactions. (a) Shows the change in column-integrated reaction rates. (b) Fractional contribution of each species + OH reaction to the additional OH loss. CO + OH is as significant as isoprene + OH on a global scale, and its delayed peak relative to isoprene + OH's peak is due to CO's longer lifetime relative to other VOCs in the cascade.

budget, and that isoprene oxidation can contribute 50%–80% of total CO chemical production in and downwind of isoprene source regions (Holloway et al., 2000; Pfister et al., 2008). Outside of isoprene and CO, other VOCs produced downstream of isoprene oxidation, such as methyl vinyl ketone (MVK) and methacrolein (MACR), also significantly impact the net OH loss, with these additional oxidation products accounting for up to 30% of the OH loss during boreal summer.

CO's contribution to the global OH decrease exceeds that of isoprene itself, and the timing lags the isoprene + OH reaction, as CO is produced downstream and has a lifetime of 1 month. This increased CO can be transported over longer distances than isoprene (Figure S10 in Supporting Information S1), which allows isoprene to have an impact on the global atmospheric oxidative capacity—beyond only affecting OH locally over isoprene source regions. Since much of intermodel variability in [OH] predictions is caused by variability in the oxidation efficiency, which is the fraction of a VOC (e.g., isoprene) oxidized to CO, the OH loss from isoprene emissions is likely sensitive to a model's isoprene and VOC oxidation mechanism (Murray et al., 2021).

Increased isoprene oxidation increases the abundance of CO in the model, raising the question: “do independent observations of CO support this increased burden?” To assess this question, we compared the model simulations to MOPITT satellite observations of CO. Figure 3 shows the globally averaged CO concentrations from MOPITT,

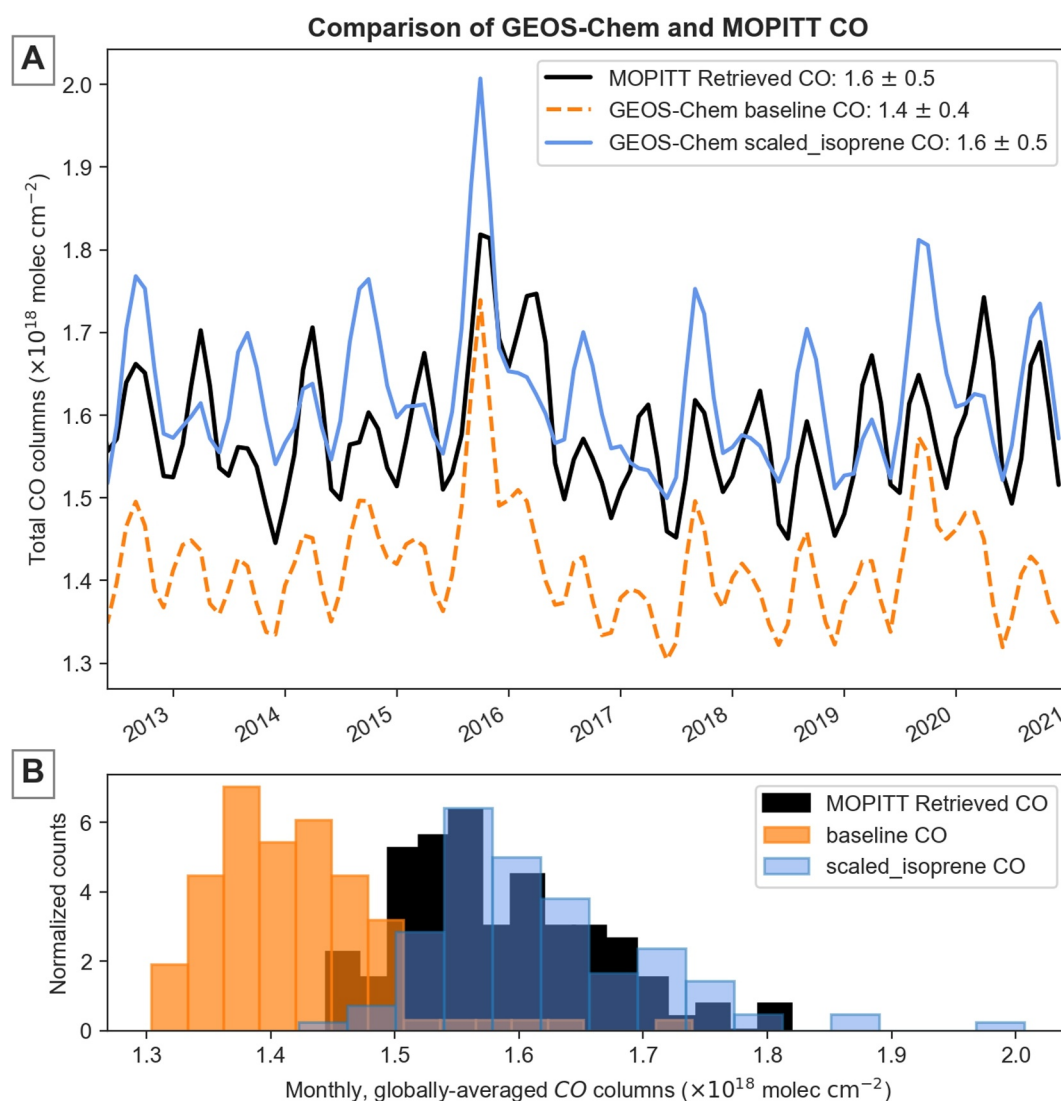


**Figure 3.** Comparison of carbon monoxide from GEOS-Chem and MOPITT. (a) Time-series of globally averaged CO columns processed through the MOPITT averaging kernel from the baseline and scaled\_isoprene GEOS-Chem runs, compared to the MOPITT total daytime CO columns. The enhanced isoprene from the scaled run translated to a CO mean that was more in alignment with MOPITT than the base run. Uncertainties are reported as 1 standard deviation. (b) Histogram of monthly, globally averaged CO columns. The difference in CO columns between both GEOS-Chem runs and the MOPITT CO retrievals was statistically significant ( $p < 0.05$ ), but the mean CO is closer in agreement with MOPITT retrievals in the scaled\_isoprene simulation than the baseline simulation.

the baseline simulation, and the scaled\_isoprene simulation. As with isoprene, the baseline simulation underpredicts MOPITT CO observations, while scaled\_isoprene shows better agreement with MOPITT retrievals. Although the bias in mean CO is detectable from observations, attributing observed interannual variability in CO to isoprene emissions is difficult, as most of the CO interannual variability (10% of annual burden) is caused by biomass-burning variability in South America and equatorial Asia, two regions with high isoprene emissions (Duncan et al., 2003; Voulgarakis et al., 2015). However, in 2019 and 2020, we see an increase in the late-year (November–January) MOPITT CO seasonal minima relative to previous years, which is when isoprene-derived CO has the highest impact on global OH oxidation (Figure 2).

Interestingly, our isoprene scaling also decreased the interhemispheric OH ratio, with the boundary-layer NH:SH [OH] ratio decreasing from 1.17 in baseline to 1.12 in scaled\_isoprene (1.15–1.13 in tropospheric [OH]). Chemistry-climate models systematically underestimate CO in the Northern Hemisphere and simulate

interhemispheric ratios above 1 (Strode et al., 2015). The elevated NH isoprene and CO concentrations in our `scaled_isoprene` run partially addresses this underestimation and brings the interhemispheric OH ratio closer to the parity observed by Patra et al. (2014).

The improved agreement between carbon monoxide from MOPITT and GEOS-Chem and the lower interhemispheric OH ratio support our isoprene scaling. Although discrepancies in the CO seasonal cycle indicate some error in the isoprene scaling, the increase in CO is plausible given independent satellite measurements.

### 3.2. Impact on Methane Growth

As mentioned above, 2020 and 2021 exhibited the largest methane growth rates ever observed in the in situ record going back to 1983; as such, there has been much speculation about what caused this methane acceleration. For 2020, offline MEGAN emissions predicted a global 12 Tg decrease in isoprene emissions relative to 2019, while our scaling indicates a 23 Tg increase, with most of this increase occurring in the Amazon and Maritime Continent. Consequently, we find a 0.6% decrease in global boundary layer [OH] from 2019 to 2020 in `scaled_isoprene` compared to `isoprene_climatology`, while the baseline simulation shows a 0.4% increase in [OH]. We attribute these modeled [OH] changes to interannual isoprene variations and the subsequent oxidation cascade.

To quantify how this change in tropospheric [OH] impacts atmospheric methane concentrations, we implemented a stepwise [OH] change into a two-box  $\text{CH}_4$ -OH model originally developed by Turner et al. (2017). This stepwise change in the two-box model was set as the percent change in hemispheric [OH] columns between 2019 and 2020 in the `scaled_isoprene` GEOS-Chem simulation. We then compared the change in methane diagnosed from the two-box model to that caused by the 1.6% decrease in tropospheric OH from Peng et al., and similarly found that a 1.6% decrease in OH explained approximately half of the methane growth in our two-box model. A theoretical 3% decrease in OH was able to explain all of 2020's methane growth, as it captured the maximum magnitude of methane growth in both hemispheres during the 2020–2021 period (Figure S11 in Supporting Information S1). Relative to the 3% [OH] decrease, we find that isoprene alone could account for 13% of the methane growth (bounds: 10%–28%) if the anomalously high isoprene columns observed in 2020 were solely driven by isoprene emissions (Figure S12 in Supporting Information S1).

Our results assume that 2020's isoprene anomalies were driven by isoprene emissions rather than changes in [OH] from  $\text{NO}_x$ , which would affect isoprene's lifetime. This assumption arises because our simulations do not consider changes in anthropogenic  $\text{NO}_x$ : modeled 2020 anthropogenic  $\text{NO}_x$  emissions were set to 2019 values. In 2020, COVID-19 lockdowns decreased tropospheric  $\text{NO}_x$  columns through lower anthropogenic emissions (Cooper et al., 2022; Venter et al., 2020), and thus some of these isoprene and OH anomalies may be due to decreasing  $\text{NO}_x$  during this period.

To address this confounding effect, we performed COVID-19 sensitivity studies that decreased anthropogenic NO emissions by the observed change in OMI  $\text{NO}_2$  columns between 2019 and 2020; these simulations are described in Text S4 of Supporting Information S1. When globally averaged, these  $\text{NO}_x$  changes could increase isoprene columns 2.5x more than what we observe from CrIS, as well as a 4x larger increase in the methane lifetime compared to the potential lifetime increase caused by isoprene emissions (Figure S13 in Supporting Information S1). However, the spatiotemporal distribution of the  $\text{NO}_x$  changes and their impact on isoprene do not match CrIS observations. For example, anthropogenic  $\text{NO}_x$  largely decreased in the Northern Hemisphere mid-latitudes, which is not spatially co-located with the large tropical isoprene sources found in this study (Figure S14 in Supporting Information S1) (Nickolay A. Krotkov et al., 2019). Although changes in  $\text{NO}_x$  may propagate over long distances through peroxyacetyl nitrates (PANs), the impact of these  $\text{NO}_x$  decreases on isoprene columns is mostly restricted to areas near large cities in the tropics, such as Bogotá, Singapore, and Jakarta. Furthermore, the isoprene anomaly remains elevated throughout the year and even peaks in the later half of the year in the Maritime Continent, while the largest COVID-19  $\text{NO}_x$  decreases were during the first half of the year, especially April–May 2020 (Laughner et al., 2021; Miyazaki et al., 2021). Nevertheless, identifying the cause of this 2020 isoprene anomaly is crucial, as it determines the mechanism through which [OH] impacts methane lifetimes. If  $\text{NO}_x$  caused elevated isoprene columns, the isoprene enhancements would not be the cause of the methane lifetime increase, but rather a symptom of the  $\text{NO}_x$  changes.



Alternatively, changes in natural  $\text{NO}_x$  sources not directly related to the COVID-19 lockdowns, like soil or lightning  $\text{NO}_x$ , can impact isoprene columns in areas like the Maritime Continent. Formaldehyde and isoprene consistently show a negative correlation in the Maritime Continent throughout the entire 8-year period, which may indicate variability caused by a non-anthropogenic  $\text{NO}_x$  source (Figure S17 in Supporting Information S1). More work needs to be done to determine the sensitivity of isoprene columns to each  $\text{NO}_x$  source (Text S5 in Supporting Information S1). Nevertheless, even if  $\text{NO}_x$  drove 2020's isoprene column anomalies, the magnitude of the OH perturbation is still sensitive to isoprene concentrations due to changes in chemistry (Wolfe et al., 2016). The 2019–2020 increase in methane lifetime with the same COVID-19  $\text{NO}_x$  perturbation was 20% higher in the *scaled\_isoprene* run than the baseline run, indicating that higher mean global isoprene emissions may amplify  $\text{NO}_x$ 's impact on [OH] (Figure S13 in Supporting Information S1). The influence of  $\text{NO}_x$  on isoprene is highly dependent on the identity of the oxidation products and thus the model's chemical mechanism. Formation of certain isoprene hydroxynitrates and their rapid hydrolysis into  $\text{HNO}_3$  may cause permanent  $\text{NO}_x$  loss in regions with changing NO emissions even with constant isoprene emissions, which impacts how the isoprene- $\text{NO}_x$  relationship affects OH and the oxidative capacity (Vasquez et al., 2020).

#### 4. Discussion

The largest isoprene anomaly in the CrIS record occurred in 2019 and 2020, coinciding with rapid methane growth. Here we investigated the hypothesis that increased isoprene emissions could indirectly contribute to this methane acceleration by modulating [OH] and CO. We scaled GEOS-Chem's offline MEGAN isoprene emissions to better match novel CrIS isoprene retrievals, bringing modeled and satellite isoprene closer in agreement. Our scaling increased isoprene emissions from 336–371 Tg C/year to 628–711 Tg C/year and strengthened the seasonal cycle in global isoprene columns. Since GEOS-Chem underestimated isoprene relative to CrIS retrievals, our results suggest that previous isoprene emission inventories may be too low. This bias is partially caused by systematically high modeled OH compared to MCF proxies, but systematic low biases in satellite formaldehyde retrievals, an isoprene proxy, compared to in situ measurements could also have caused underestimated isoprene fluxes in previous studies (Müller et al., 2024; Zhu et al., 2016).

Increased isoprene—and increased CO from the isoprene oxidation cascade—resulted in longer methane lifetimes due to decreased [OH]. This scaling improved agreement between MOPITT CO and the *scaled\_isoprene* run's CO and lowered the interhemispheric OH ratio closer to parity. Through a combination of 0D and 3D atmospheric modeling, we show that the isoprene increase observed by CrIS during 2020 could account for 13% of 2020's methane acceleration. We obtain this value while using 2019 anthropogenic NO emissions as 2020 NO fluxes, and thus this value represents the potential impact of isoprene on 2020's methane acceleration assuming no contribution from  $\text{NO}_x$  changes.

Determining the causality of this isoprene anomaly is crucial in quantifying the [OH] response. Here, we investigate the implications of an isoprene anomaly driven solely by isoprene emissions as a potential hypothesis, but  $\text{NO}_x$  and other drivers of [OH] (e.g., actinic flux) also can influence isoprene columns observed from space. If this 2020 isoprene anomaly were driven by decreasing  $\text{NO}_x$  emissions, the observed changes in isoprene columns would be a response to the independently changing oxidative capacity, rather than isoprene being the causal agent for the [OH] changes. This different causality may influence the magnitude of the resulting [OH] perturbation, but the nonlinear relationship of the isoprene–OH– $\text{NO}_x$  system warrants further investigation.

Although 2020 is a special year of interest due to the methane acceleration and the potential discrepancy between MEGAN isoprene emissions and observed columns, other years within the record also experienced comparable isoprene anomalies to 2020's anomalies without similarly large perturbations to anthropogenic  $\text{NO}_x$ . Thus, the potential magnitude of these interannual variations in isoprene and their resulting impacts on [OH] are not contingent on the accuracy of our isoprene emission scaling, although our scaling can change when these variations occur. For example, even in the baseline simulation with MEGAN-generated isoprene emissions, variations in isoprene emissions caused a 0.5% decrease in global [OH] between 2014 and 2015, and a 0.1% decrease in [OH] between 2015 and 2016. Given that a 1.6% decrease in [OH] may have contributed to the unprecedented methane growth in 2020, isoprene may be an important but overlooked factor in explaining recent methane trends. We also note that GEOS-Chem underestimates this observed variability (Figure S4 in Supporting Information S1), which may in turn underestimate the resulting OH impacts.

This study illustrates how isoprene can impact the global atmospheric oxidative capacity and methane lifetimes. We suggest that variations in isoprene, and thus changes to the biosphere, may have an important effect on the atmospheric oxidative capacity, although more research is needed to fully attribute these 2020 observations to increased isoprene emissions, decreased  $\text{NO}_x$  emissions, or changes in isoprene- $\text{NO}_x$  chemistry. Given that isoprene emissions are driven by short-term meteorological conditions, climate oscillations like ENSO, and long-term climate change, this mechanism may represent a potential interaction between the biosphere and the climate system mediated through atmospheric chemistry.

## Data Availability Statement

All model output, the two-box model source code, and the monthly global CrIS retrievals used in this study are published in Yoon et al. (2025).

## Acknowledgments

This research received support from the generosity of Eric and Wendy Schmidt by recommendation of Schmidt Sciences through the VESRI program. JAT acknowledges support from the National Science Foundation (AGS-2023670). ALSS acknowledges support from the National Science Foundation award number DEB-1925837. DBM and KCW acknowledge support from NASA (Grant 80NSSC24M0037).

## References

- Bamberger, I., Ruehr, N. K., Schmitt, M., Gast, A., Wohlfahrt, G., & Arneth, A. (2017). Isoprene emission and photosynthesis during heatwaves and drought in black locust. *Biogeosciences*, 14(15), 3649–3667. <https://doi.org/10.5194/bg-14-3649-2017>
- Bates, K. H., & Jacob, D. J. (2019). A new model mechanism for atmospheric oxidation of isoprene: Global effects on oxidants, nitrogen oxides, organic products, and secondary organic aerosol. *Atmospheric Chemistry and Physics*, 19(14), 9613–9640. <https://doi.org/10.5194/acp-19-9613-2019>
- Cooper, M. J., Martin, R. V., Hammer, M. S., Levelt, P. F., Veefkind, P., Lamsal, L. N., et al. (2022). Global fine-scale changes in ambient  $\text{NO}_2$  during COVID-19 lockdowns. *Nature*, 601(7893), 380–387. <https://doi.org/10.1038/s41586-021-04229-0>
- Duncan, B. N., Martin, R. V., Staudt, A. C., Yevich, R., & Logan, J. A. (2003). Interannual and seasonal variability of biomass burning emissions constrained by satellite observations. *Journal of Geophysical Research*, 108(D2), ACH 22. <https://doi.org/10.1029/2002JD002378>
- Emmons, L. K., Schwantes, R. H., Orlando, J. J., Tyndall, G., Kinnison, D., Lamarque, J.-F., et al. (2020). The chemistry mechanism in the Community Earth System Model version 2 (CESM2). *Journal of Advances in Modeling Earth Systems*, 12(4), e2019MS001882. <https://doi.org/10.1029/2019MS001882>
- Feng, L., Palmer, P. I., Parker, R. J., Lunt, M. F., & Bösch, H. (2023). Methane emissions are predominantly responsible for record-breaking atmospheric methane growth rates in 2020 and 2021. *Atmospheric Chemistry and Physics*, 23(8), 4863–4880. <https://doi.org/10.5194/acp-23-4863-2023>
- Guenther, A., Karl, T., Harley, P., Wiedinmyer, C., Palmer, P. I., & Geron, C. (2006). Estimates of global terrestrial isoprene emissions using MEGAN (model of emissions of gases and aerosols from nature). *Atmospheric Chemistry and Physics*, 6(11), 3181–3210. <https://doi.org/10.5194/acp-6-3181-2006>
- Guenther, A. B., Jiang, X., Heald, C. L., Sakulyanontvittaya, T., Duhl, T., Emmons, L. K., & Wang, X. (2012). The Model of Emissions of Gases and Aerosols from Nature version 2.1 (MEGAN2.1): An extended and updated framework for modeling biogenic emissions. *Geoscientific Model Development*, 5(6), 1471–1492. <https://doi.org/10.5194/gmd-5-1471-2012>
- Hardy, A., Palmer, P. I., & Oakes, G. (2023). Satellite data reveal how Sudd wetland dynamics are linked with globally-significant methane emissions. *Environmental Research Letters*, 18(7), 074044. <https://doi.org/10.1088/1748-9326/ace272>
- Holloway, T., Levy, H. II., & Kasibhatla, P. (2000). Global distribution of carbon monoxide. *Journal of Geophysical Research*, 105(D10), 12123–12147. <https://doi.org/10.1029/1999JD901173>
- Kroll, J. H., Ng, N. L., Murphy, S. M., Flagan, R. C., & Seinfeld, J. H. (2006). Secondary organic aerosol formation from isoprene photooxidation. *Environmental Science and Technology*, 40(6), 1869–1877. <https://doi.org/10.1021/es0524301>
- Krotkov, N. A., Lamsal, L. N., Marchenko, S. V., Celarier, E. A., Bucsela, E. J., Swartz, W. H., et al. (2019). OMI/Aura  $\text{NO}_2$  cloud-screened total and tropospheric column L3 global gridded 0.25 degree x 0.25 degree V3 [Dataset]. NASA Goddard Space Flight Center, Goddard Earth Sciences Data and Information Services Center (GES DISC). <https://doi.org/10.5067/Aura/OMI/DATA3007>
- Lan, X., Mund, J., Crotwell, A., Thoning, K., Moglia, E., Madronich, M., et al. (2024). Atmospheric methane dry air mole fractions from the NOAA GML carbon cycle cooperative global air sampling network, 1983–2024 [Dataset]. <https://doi.org/10.15138/VNCZ-M766>
- Laughner, J. L., Neu, J. L., Schimel, D., Wennberg, P. O., Barsanti, K., Bowman, K. W., et al. (2021). Societal shifts due to COVID-19 reveal large-scale complexities and feedbacks between atmospheric chemistry and climate change. *Proceedings of the National Academy of Sciences*, 118(46), e2109481118. <https://doi.org/10.1073/pnas.2109481118>
- Lin, H., Emmons, L. K., Lundgren, E. W., Yang, L. H., Feng, X., Dang, R., et al. (2024). Intercomparison of GEOS-Chem and CAM-chem tropospheric oxidant chemistry within the Community Earth System Model version 2 (CESM2). *Atmospheric Chemistry and Physics*, 24(15), 8607–8624. <https://doi.org/10.5194/acp-24-8607-2024>
- Millet, D. B., Jacob, D. J., Turquety, S., Hudman, R. C., Wu, S., Fried, A., et al. (2006). Formaldehyde distribution over North America: Implications for satellite retrievals of formaldehyde columns and isoprene emission. *Journal of Geophysical Research*, 111(D24). <https://doi.org/10.1029/2005JD006853>
- Millet, D. B., Jacob, D. J., Boersma, K. F., Fu, T.-M., Kurosu, T. P., Chance, K., et al. (2008). Spatial distribution of isoprene emissions from North America derived from formaldehyde column measurements by the OMI satellite sensor. *Journal of Geophysical Research*, 113(D2). <https://doi.org/10.1029/2007JD008950>
- Miyazaki, K., Bowman, K., Sekiya, T., Takigawa, M., Neu, J. L., Sudo, K., et al. (2021). Global tropospheric ozone responses to reduced  $\text{NO}_x$  emissions linked to the COVID-19 worldwide lockdowns. *Science Advances*, 7(24), eabf7460. <https://doi.org/10.1126/sciadv.abf7460>
- Müller, J.-F., Stavrou, T., Oomen, G.-M., Opacka, B., De Smedt, I., Guenther, A., et al. (2024). Bias correction of OMI HCHO columns based on FTIR and aircraft measurements and impact on top-down emission estimates. *Atmospheric Chemistry and Physics*, 24(4), 2207–2237. <https://doi.org/10.5194/acp-24-2207-2024>
- Murray, L. T., Fiore, A. M., Shindell, D. T., Naik, V., & Horowitz, L. W. (2021). Large uncertainties in global hydroxyl projections tied to fate of reactive nitrogen and carbon. *Proceedings of the National Academy of Sciences*, 118(43), e2115204118. <https://doi.org/10.1073/pnas.2115204118>

- Nguyen, N. H., Turner, A. J., Yin, Y., Prather, M. J., & Frankenberg, C. (2020). Effects of chemical feedbacks on decadal methane emissions estimates. *Geophysical Research Letters*, 47(3), e2019GL085706. <https://doi.org/10.1029/2019GL085706>
- Palmer, P. I., Jacob, D. J., Fiore, A. M., Martin, R. V., Chance, K., & Kurosu, T. P. (2003). Mapping isoprene emissions over North America using formaldehyde column observations from space. *Journal of Geophysical Research*, 108(D6). <https://doi.org/10.1029/2002JD002153>
- Palmer, P. I., Abbot, D. S., Fu, T.-M., Jacob, D. J., Chance, K., Kurosu, T. P., et al. (2006). Quantifying the seasonal and interannual variability of North American isoprene emissions using satellite observations of the formaldehyde column. *Journal of Geophysical Research*, 111(D12). <https://doi.org/10.1029/2005JD006689>
- Patra, P. K., Krol, M. C., Montzka, S. A., Arnold, T., Atlas, E. L., Lintner, B. R., et al. (2014). Observational evidence for interhemispheric hydroxyl-radical parity. *Nature*, 513(7517), 219–223. <https://doi.org/10.1038/nature13721>
- Peng, S., Lin, X., Thompson, R. L., Xi, Y., Liu, G., Hauglustaine, D., et al. (2022). Wetland emission and atmospheric sink changes explain methane growth in 2020. *Nature*, 612(7940), 477–482. <https://doi.org/10.1038/s41586-022-05447-w>
- Pfister, G. G., Emmons, L. K., Hess, P. G., Lamarque, J.-F., Orlando, J. J., Walters, S., et al. (2008). Contribution of isoprene to chemical budgets: A model tracer study with the NCAR CTM MOZART-4. *Journal of Geophysical Research*, 113(D5). <https://doi.org/10.1029/2007JD008948>
- Rigby, M., Montzka, S. A., Prinn, R. G., White, J. W. C., Young, D., O'Doherty, S., et al. (2017). Role of atmospheric oxidation in recent methane growth. *Proceedings of the National Academy of Sciences*, 114(21), 5373–5377. <https://doi.org/10.1073/pnas.1616426114>
- Saunio, M., Stavert, A. R., Poulter, B., Bousquet, P., Canadell, J. G., Jackson, R. B., et al. (2020). The global methane budget 2000–2017. *Earth System Science Data*, 12(3), 1561–1623. <https://doi.org/10.5194/essd-12-1561-2020>
- Shutter, J. D., Millet, D. B., Wells, K. C., Payne, V. H., Nowlan, C. R., & Abad, G. G. (2024). Interannual changes in atmospheric oxidation over forests determined from space. *Science Advances*, 10(20), eadn1115. <https://doi.org/10.1126/sciadv.adn1115>
- Smith, C., Nicholls, Z. R. J., Armour, K., Collins, W., Forster, P., Meinshausen, M., et al. (2021). The Earth's energy budget, climate feedbacks, and climate sensitivity. *Supplementary Material (Tech. Rep.)*. Retrieved from [https://www.ipcc.ch/report/ar6/wg1/downloads/report/IPCC\\_AR6\\_WGI\\_Chapter07\\_SM.pdf](https://www.ipcc.ch/report/ar6/wg1/downloads/report/IPCC_AR6_WGI_Chapter07_SM.pdf)
- Strode, S. A., Duncan, B. N., Yegorova, E. A., Kouatchou, J., Ziemke, J. R., & Douglass, A. R. (2015). Implications of carbon monoxide bias for methane lifetime and atmospheric composition in chemistry climate models. *Atmospheric Chemistry and Physics*, 15(20), 11789–11805. <https://doi.org/10.5194/acp-15-11789-2015>
- Turner, A. J., Henze, D. K., Martin, R. V., & Hakami, A. (2012). The spatial extent of source influences on modeled column concentrations of short-lived species. *Geophysical Research Letters*, 39(12). <https://doi.org/10.1029/2012GL051832>
- Turner, A. J., Frankenberg, C., Wennberg, P. O., & Jacob, D. J. (2017). Ambiguity in the causes for decadal trends in atmospheric methane and hydroxyl. *Proceedings of the National Academy of Sciences*, 114(21), 5367–5372. <https://doi.org/10.1073/pnas.1616020114>
- Vasquez, K. T., Crounse, J. D., Schulze, B. C., Bates, K. H., Teng, A. P., Xu, L., et al. (2020). Rapid hydrolysis of tertiary isoprene nitrate efficiently removes NO<sub>x</sub> from the atmosphere. *Proceedings of the National Academy of Sciences*, 117(52), 33011–33016. <https://doi.org/10.1073/pnas.2017442117>
- Velikova, V., Várkonyi, Z., Szabó, M., Maslenkova, L., Nogues, I., Kovács, L., et al. (2011). Increased thermostability of thylakoid membranes in isoprene-emitting leaves probed with three biophysical techniques. *Plant Physiology*, 157(2), 905–916. <https://doi.org/10.1104/pp.111.182519>
- Venter, Z. S., Aunan, K., Chowdhury, S., & Lelieveld, J. (2020). COVID-19 lockdowns cause global air pollution declines. *Proceedings of the National Academy of Sciences*, 117(32), 18984–18990. <https://doi.org/10.1073/pnas.2006853117>
- Voulgarakis, A., Marlier, M. E., Faluvegi, G., Shindell, D. T., Tsigaridis, K., & Mangeon, S. (2015). Interannual variability of tropospheric trace gases and aerosols: The role of biomass burning emissions. *Journal of Geophysical Research: Atmospheres*, 120(14), 7157–7173. <https://doi.org/10.1002/2014JD022926>
- Wells, K. C., Millet, D. B., Payne, V. H., Deventer, M. J., Bates, K. H., de Gouw, J. A., et al. (2020). Satellite isoprene retrievals constrain emissions and atmospheric oxidation. *Nature*, 585(7824), 225–233. <https://doi.org/10.1038/s41586-020-2664-3>
- Wells, K. C., Millet, D. B., Payne, V. H., Vigouroux, C., Aquino, C. A. B., De Mazière, M., et al. (2022). Next-generation isoprene measurements from space: Detecting daily variability at high resolution. *Journal of Geophysical Research: Atmospheres*, 127(5), e2021JD036181. <https://doi.org/10.1029/2021JD036181>
- Wolfe, G. M., Kaiser, J., Hanisco, T. F., Keutsch, F. N., de Gouw, J. A., Gilman, J. B., et al. (2016). Formaldehyde production from isoprene oxidation across NO<sub>x</sub> regimes. *Atmospheric Chemistry and Physics*, 16(4), 2597–2610. <https://doi.org/10.5194/acp-16-2597-2016>
- Yoon, J., Wells, K. C., Millet, D. B., Swann, A. L., Thornton, J., & Turner, A. J. (2025). Data from: Impacts of interannual isoprene variations on methane lifetimes and trends [Dataset]. *Zenodo*. <https://doi.org/10.5281/zenodo.14020788>
- Zhao, Y., Saunio, M., Bousquet, P., Lin, X., Hegglin, M. I., Canadell, J. G., et al. (2023). Reconciling the bottom-up and top-down estimates of the methane chemical sink using multiple observations. *Atmospheric Chemistry and Physics*, 23(1), 789–807. <https://doi.org/10.5194/acp-23-789-2023>
- Zheng, Y., Unger, N., Tadić, J. M., Seco, R., Guenther, A. B., Barkley, M. P., et al. (2017). Drought impacts on photosynthesis, isoprene emission and atmospheric formaldehyde in a mid-latitude forest. *Atmospheric Environment*, 167, 190–201. <https://doi.org/10.1016/j.atmosenv.2017.08.017>
- Zhu, L., Jacob, D. J., Kim, P. S., Fisher, J. A., Yu, K., Travis, K. R., et al. (2016). Observing atmospheric formaldehyde (HCHO) from space: Validation and intercomparison of six retrievals from four satellites (OMI, GOME2A, GOME2B, OMPS) with SEAC<sup>4</sup>RS aircraft observations over the southeast US. *Atmospheric Chemistry and Physics*, 16(21), 13477–13490. <https://doi.org/10.5194/acp-16-13477-2016>

## References From the Supporting Information

- Chance, K. (2024). OMI/Aura formaldehyde (HCHO) total column daily L3 weighted mean global 0.1deg Lat/Lon grid [Dataset]. *Goddard Earth Sciences Data and Information Services Center (GES DISC)*. <https://doi.org/10.5067/Aura/OMI/DATA3010>
- Fu, D., Millet, D. B., Wells, K. C., Payne, V. H., Yu, S., Guenther, A., & Eldering, A. (2019). Direct retrieval of isoprene from satellite-based infrared measurements. *Nature Communications*, 10(1), 3811. <https://doi.org/10.1038/s41467-019-11835-0>
- González Abad, G., Liu, X., Chance, K., Wang, H., Kurosu, T. P., & Suleiman, R. (2015). Updated Smithsonian Astrophysical Observatory Ozone Monitoring instrument (SAO OMI) formaldehyde retrieval. *Atmospheric Measurement Techniques*, 8(1), 19–32. <https://doi.org/10.5194/amt-8-19-2015>
- Li, Y., Zhu, Y., Tan, J. Y. K., Teo, H. C., Law, A., Qu, D., & Luo, W. (2022). The impact of COVID-19 on NO<sub>2</sub> and PM<sub>2.5</sub> levels and their associations with human mobility patterns in Singapore. *Annals of GIS*, 28(4), 515–531. <https://doi.org/10.1080/19475683.2022.2121855>
- Murray, L. T. (2016). Lightning NO<sub>x</sub> and impacts on air quality. *Current Pollution Reports*, 2(2), 115–133. <https://doi.org/10.1007/s40726-016-0031-7>

- NASA/LARC/SD/ASDC. (2023). MOPITT CO gridded monthly means (near and thermal infrared radiances) V009 [Dataset]. *NASA Langley Atmospheric Science Data Center DAAC*. <https://doi.org/10.5067/TERRA/MOPITT/MOP03JM.009>
- Sun, K., Zhu, L., Cady-Pereira, K., Chan Miller, C., Chance, K., Clarisse, L., et al. (2018). A physics-based approach to oversample multi-satellite, multispecies observations to a common grid. *Atmospheric Measurement Techniques*, 11(12), 6679–6701. <https://doi.org/10.5194/amt-11-6679-2018>
- Thornton, J. A., Virts, K. S., Holzworth, R. H., & Mitchell, T. P. (2017). Lightning enhancement over major oceanic shipping lanes. *Geophysical Research Letters*, 44(17), 9102–9111. <https://doi.org/10.1002/2017GL074982>
- Yuan, T., Song, H., Wood, R., Wang, C., Oreopoulos, L., Platnick, S. E., et al. (2022). Global reduction in ship-tracks from sulfur regulations for shipping fuel. *Science Advances*, 8(29), eabn7988. <https://doi.org/10.1126/sciadv.abn7988>